

# Efficient Generation of Microwave Plasmonic Vortices via a Single Deep-Subwavelength Meta-Particle

Hai Su, Xiaopeng Shen, Guangxu Su, Lin Li, Jianping Ding, Fanxin Liu, Peng Zhan,\*  
Yongmin Liu,\* and Zhenlin Wang\*

Light beams carrying orbital angular momentum (OAM) in the form of optical vortices have attracted great interest due to their capability for providing a new dimension and approach to manipulate light–matter interactions. Recently, plasmonics has offered efficient ways to focus vortex beams beyond the diffraction limit. However, unlike in the visible and near-infrared regime, it is still a big challenge to realize plasmonic vortices at far-infrared and even longer wavelengths. An effective strategy to create deep-subwavelength near-field electromagnetic (EM) vortices operating in the low frequency region is proposed. Taking advantage of the asymmetric spatial distribution of EM field supported by a metallic comb-shaped waveguide, plasmonic vortex modes that are strongly confined in a well-designed deep-subwavelength meta-particle with desired topological charges can be excited. Such unique phenomena are confirmed by the microwave experiments. An equivalent physical model backed up by the numerical simulations is performed to reveal the underlying mechanism of the plasmonic vortex generation. This spoof-plasmon assisted focusing of EM waves with OAM may find potentials for functional integrated elements and devices operating in the microwave, terahertz, and even far-infrared regions.

referred to as optical vortices, which have found many applications such as micro-manipulation,<sup>[6]</sup> imaging,<sup>[7]</sup> data storage,<sup>[8]</sup> high-capacity communication,<sup>[9]</sup> and even quantum cryptography.<sup>[10]</sup> In free-space optics, vortex beams could be generated through conventional mode conversion of Gaussian beams by using the bulky devices, including spiral phase plates,<sup>[4,5]</sup> spatial light modulators,<sup>[11,12]</sup> and computer-generated holograms.<sup>[13]</sup> More interestingly, some new strategies have been demonstrated to generate OAM beams using artificial microstructures such as phase-controlled metasurfaces<sup>[14–17]</sup> and angular grating embedded ring-resonators,<sup>[18,19]</sup> which are adopted to meet the requirement for miniaturization and integration of optical devices.

Due to the diffraction limit, the radius of free space OAM modes is usually comparable to the excitation wavelength. Recently, plasmonic vortices<sup>[20–25]</sup>

## 1. Introduction

As one of the most fundamental physical quantities, angular momentum of light has made enormous progress in recent years. Optical angular momentum can be categorized into spin angular momentum (SAM)<sup>[1,2]</sup> and orbital angular momentum (OAM).<sup>[3–5]</sup> SAM is associated with circular polarization of light, which takes the value of  $+\hbar$  (right-circularly polarized light) or  $-\hbar$  (left-circularly polarized light). OAM is related to optical paraxial beams possessing helical phase fronts, also usually


have provided a potential way to generate OAM modes beyond the diffraction limit. Typically, these plasmonic vortices refer to surface plasmon polaritons (SPPs) with a dark spot and phase singularity at its center, which can strongly confine OAM information in the evanescent field region with subwavelength dimensions. In order to generate plasmonic vortices with specific topological charges, flat metal surfaces are usually decorated with some pragmatically designed structures such as Archimedean spirals<sup>[20–23]</sup> and related nanostructures,<sup>[24,25]</sup> which play the roles of exciting SPPs and regulating their phase gradient

H. Su, G. Su, Prof. J. Ding, Prof. F. Liu, Prof. P. Zhan, Prof. Z. Wang  
School of Physics  
National Laboratory of Solid State Microstructures and Collaborative  
Innovation Center of Advanced Microstructures  
Nanjing University  
Nanjing 210093, China  
E-mail: zhanpeng@nju.edu.cn; zlwang@nju.edu.cn

Prof. X. Shen  
School of Physical Science and Technology  
China University of Mining and Technology  
Xuzhou 221116, China

Dr. L. Li, Prof. Y. Liu  
Department of Mechanical and Industrial Engineering and Department  
of Electrical and Computer Engineering  
Northeastern University  
Boston, MA 02115, USA  
E-mail: y.liu@northeastern.edu

Prof. F. Liu  
Department of Applied Physics  
Zhejiang University of Technology  
Xiaoheshan, Hangzhou 310023, China

 The ORCID identification number(s) for the author(s) of this article can be found under <https://doi.org/10.1002/lpor.201800010>

DOI: 10.1002/lpor.201800010

simultaneously. However, the effective excitation of SPPs severely relies on the penetration of electromagnetic (EM) field into metals, and thus these plasmonic vortices are inevitably limited to visible and near-infrared frequencies. At low frequencies (i.e., microwave, terahertz, or far-infrared), metals behave like perfect electric conductors (PECs), and thus they are unable to support SPPs. To overcome this barrier, the concept of spoof SPPs<sup>[26]</sup> has been developed by using structured metal surfaces to confine EM modes, in analogy to SPPs at visible and near-infrared frequencies.<sup>[26–37]</sup>

In this work, we propose an effective way to generate deep-subwavelength near-field EM vortex modes working at low frequencies. Taking advantage of the asymmetric spatial distribution of EM field supported by a metallic comb-shaped waveguide, spoof plasmonic vortices with desired topological charges supported by a well-designed meta-particle can be selectively excited. Moreover, an equivalent physical model backed up by the numerical simulations is performed to describe the EM field transfer characteristics and reveal the underlying mechanism for the generation of plasmonic vortex modes. Microwave experiments, including the S-parameters and the near-field characterizations, are performed to demonstrate our design, which agree with the numerical simulations and the equivalent model very well. It is worthwhile to note that the equivalent radius of the near-field EM vortex equals 1/16 of the corresponding free space wavelength. Our work provides an effective way to confine OAM-carrying EM mode to a deep-subwavelength scale, which could be very useful for integrated compact elements and devices operating in the far-infrared, terahertz, or microwave regions.

## 2. Electric Dipole Resonance of a Meta-Particle

Metallic spiral-based structures have been widely used in the design of metamaterials due to their unique EM responses. In this study, considering the strong confinement of the EM field at the resonance frequency, we employ a meta-particle comprising six long-spiral PEC arms,<sup>[33,35–37]</sup> as shown the insets of Figure 1a. Here, as an example, the equivalent radius ( $R$ ) and thickness ( $t$ ) of this meta-particle are set as 1.81 mm and 0.018 mm, respectively. The meta-particle is placed on a 0.5 mm-thick ( $d$ ) dielectric layer with a relative permittivity of 2.55. More detailed information about the geometry of this meta-particle is provided in Figure S1 of the Supporting Information. The EM response of this meta-particle can be described by the simulated extinction cross section as a function of the frequency depicted in Figure 1a, which is calculated by using the commercial software CST Microwave Studio. In the simulation, a linearly polarized plane wave propagates along the  $x$ -direction, and the electric field points along the  $y$ -direction. An obvious extinction peak is observed at 9.9 GHz, corresponding to 30.3 mm in wavelength that is 16-fold larger than the size of the meta-particle. This EM mode could be identified as a highly localized dipole resonance via the electric field distribution plotted in Figure 1b. To present the dynamic behavior of the dipole resonance during one oscillation period, the real-time evolution of the  $\text{Re}(E_z)$  are plotted as four snapshots in Figure 1b, clearly showing an equivalent electric dipole that oscillates along the  $y$ -axis. In Figure 1c, we plot the corresponding phase of

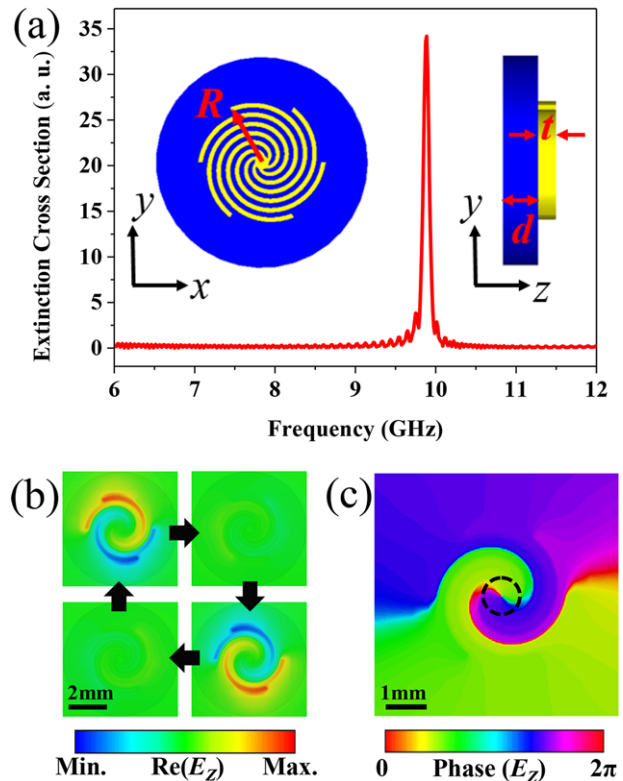


**Figure 1.** Electric dipole resonance of a meta-particle. a) Extinction cross section of the meta-particle placed on top of a dielectric layer. b) Near-field distribution, and c) phase distribution of  $E_z$  component for dipole resonance in the  $x$ - $y$  plane (0.5 mm above the meta-particle) at 9.9 GHz. The four snapshots of the near-field distribution (b) are taken at every quarter of a period.

the resonance, which exhibits a discrete phase distribution (about  $\pi/2$  and  $3\pi/2$ ) along the azimuthal direction of the meta-particle (black dashed circle).

## 3. Dispersion Relationship and High-Efficiency Conversion of Spoof SPPs

As we know, using evanescent field of a waveguide is an effective way to excite resonant modes of nanoparticles in its vicinity,<sup>[38,39]</sup> which may lead to some new resonant behaviors. For the spiral-based meta-particle, this method indeed can effectively excite the electric and magnetic localized EM modes.<sup>[37]</sup> In fact, the asymmetric spatial distribution of evanescent field has an important impact on the characteristics of localized EM modes of the meta-particle. Here, a comb-shaped PEC stripe with thickness ( $t$ ) of 0.018 mm and height ( $H$ ) of 5 mm working as spoof SPPs waveguide has been utilized, as shown in the inset of Figure 2a, which is also placed on a 0.5 mm-thick ( $d$ ) dielectric layer with a relative permittivity of 2.55. The period ( $p$ ) and width ( $a$ ) of square grooves are set as 5 mm and 2 mm, respectively. It is worthwhile to note that the dispersion of spoof SPPs is strongly dependent on the depth ( $h$ ) of grooves, as shown in Figure 2a. The nature of the spatial asymmetry of the evanescent wave provided by this comb-shaped PEC stripe is demonstrated in Figure

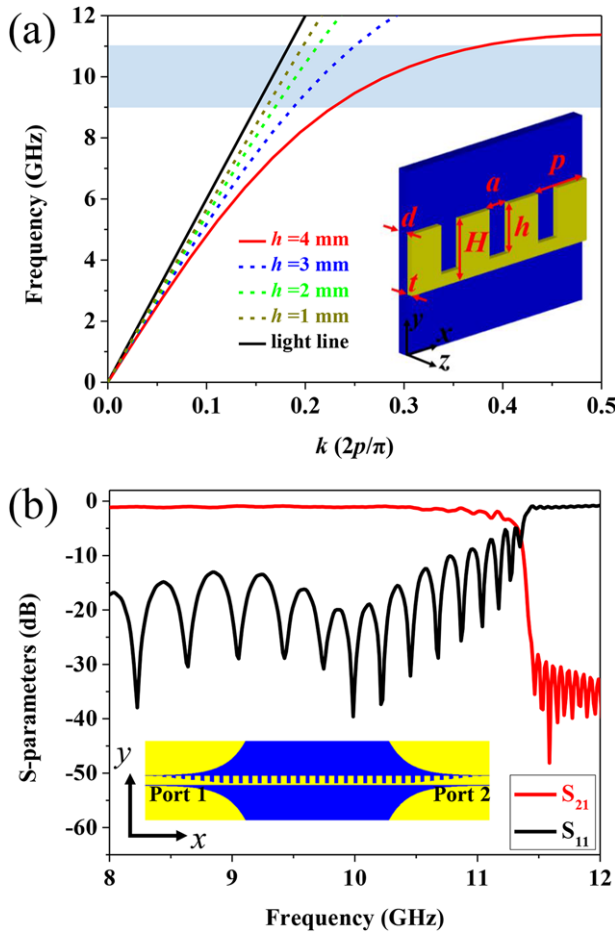


**Figure 2.** Dispersion relationship and high-efficiency conversion of spoof SPPs. a) Colorful lines represent the simulated dispersion relationship of spoof SPPs supported by comb-shaped PEC stripe with varying groove depths ( $h$ ) placed on a 0.5 mm-thick dielectric layer. b) Red and black lines represent the transmission ( $S_{21}$ ) and reflection ( $S_{11}$ ) coefficients of the hybrid waveguide (consisting of coplanar waveguides, spoof SPPs waveguide, and conversion structures), respectively.

$S_2$  of the Supporting Information. In our design, the depth ( $h$ ) of grooves is optimized as 4 mm to ensure that spoof SPPs can be more tightly confined to this comb-shaped structure within the frequency band marked with the shaded area in Figure 2a, which covers the resonant frequency of meta-particle in Figure 1a. In order to achieve high-efficiency conversion from guided waves to spoof SPPs (join the traditional coplanar waveguide with 50  $\Omega$  impedance to the comb-shaped PEC stripe), we apply a conversion structure[32] consisting of gradient corrugation grooves and flaring grounds, as shown in the inset of Figure 2b. Detailed geometric parameters of these structures are presented in Figure S3 of the Supporting Information. Within the frequency band from 9 GHz to 11GHz, such hybrid waveguide consisting of coplanar waveguides, spoof SPPs waveguide, and conversion structures has efficient transmission coefficient (red line,  $S_{21}$ ) and low reflection coefficient (black line,  $S_{11}$ ), as shown in Figure 2b. Here, we define the left (right) side of the hybrid waveguide as Port 1(2).

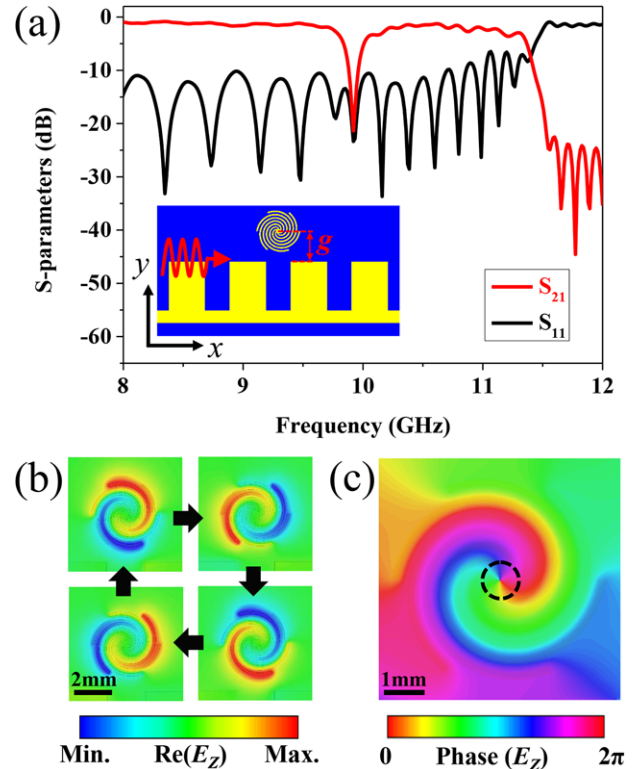


**Figure 3.** Counter-clockwise localized EM vortex (topological charge  $= -1$ ). a) Red and black lines represent the transmission ( $S_{21}$ ) and reflection ( $S_{11}$ ) coefficients of hybrid waveguide combined with the meta-particle, respectively. b) Near-field distribution, and c) helical phase distribution of  $E_z$  component for counter-clockwise vortex in the  $x$ - $y$  plane (0.5 mm above the meta-particle) at 9.9 GHz. The four snapshots of the near-field distribution (b) are taken at every quarter of a period.

#### 4. Efficient Generation of Plasmonic Vortex

To study the localized EM mode of the meta-particle excited by evanescent field, the meta-particle is placed close to the comb-shaped PEC stripe with an optimized coupling distance of  $g$  as schematically shown in the inset of Figure 3a. Based on the simulations (Figure S4, Supporting Information), the parameter of the coupling distance ( $g$ ) is determined as 2.5 mm. In this case, the coupling between spoof SPPs waveguide and the meta-particle can result in an obvious and strong suppression of the transmission at 9.9 GHz for spoof SPPs (shown in Figure 3a), which essentially satisfies the critical coupling condition and thus most energy can be coupled to the meta-particle. We numerically monitor the near-field distribution in the  $x$ - $y$  plane (0.5 mm above the meta-particle) at 9.9 GHz. Figure 3b plots the electric field distribution of the meta-particle, in which four snapshots illustrate the dynamic behavior of the localized EM vortex mode during one period (Figure S5 of the Supporting Information shows the concentrated field of the plasmonic vortex). One can clearly see that the field patterns rotate counter-clockwise. The corresponding helical phase distribution along the azimuthal direction and phase singularity are shown in Figure 3c. In a sharp contrast to Figure 1c, here the phase continuously changes from 0 to  $2\pi$  along the azimuthal direction, manifesting that the generated

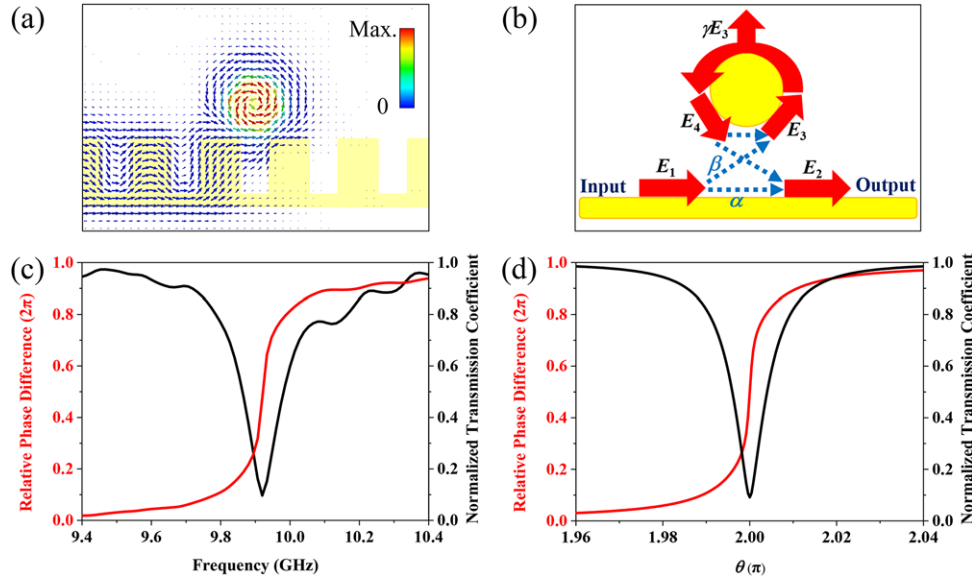


**Figure 4.** Formation mechanism of the near-field EM vortex. a) Power flow distribution of the coupled system consisting of a plasmonic waveguide and a meta-particle. b) Equivalent model revealing the mechanism of near-field EM vortex. c) Numerical calculation, and d) theoretical prediction for normalized transmission coefficient (black line) and relative phase difference (red line) of the waveguide caused by a meta-particle.

EM mode acquires OAM with topological charge  $l = -1$ . Applying the same approach, we can excite the localized vortex rotating in the clockwise direction with topological charge  $l = +1$  via switching the excitation direction of spoof SPPs, as shown in Figure S6 of the Supporting Information. By adjusting the geometric dimensions of the meta-particle, it is also possible to generate localized vortices possessing OAM of topological charge  $l = \pm 2$ , as shown in Figures S7 and S8 of the Supporting Information.

## 5. Physical Mechanism of Plasmonic Vortex

In Figure 4a, we numerically monitor the power flow distribution in the  $x$ - $y$  plane 0.5 mm above the coupled system at the response frequency of 9.9 GHz. The power flow distribution forms counter-clockwise closed loops near the meta-particle, which is under the excitation of spoof SPPs propagating from left to right. In order to reveal the formation mechanism of near-field EM vortices, we use a simplified equivalent model to describe the EM field transfer characteristics of the coupled system, which is illustrated in Figure 4b. By comparing the black-lines in Figures 2b and 3a, one can recognize that the meta-particle has negligible influence on the reflection efficiency of the hybrid waveguide, though the transmission of spoof SPPs are strongly suppressed near 9.9 GHz. Therefore, we do not consider the reflection of EM field of spoof SPPs in the equivalent model. Physically, most energy of the coupled system is trapped by the deep-subwavelength meta-particle and rotates in the form of localized vortex so that both the transmission and reflection coefficients are extremely low at 9.9 GHz. A weak radiative loss of the near-field vortex mode, in analogy of the bending loss in the dielectric ring-resonator, should be considered although it is very weak. As a result, similar to the analysis of the coupling process of fiber-ring resonators,<sup>[40–42]</sup> the

EM fields transfer in this coupled system (schematically marked as Figure 4b) satisfies the following three equations:

$$E_2 = \alpha E_1 + i\beta E_4 \quad (1)$$

$$E_3 = i\beta E_1 + \alpha E_4 \quad (2)$$

$$E_4 = (1 - \gamma)\exp(j\theta) E_3 \quad (3)$$

Here, Equations (1) and (2) describe the coupling process between the spoof SPPs mode and the near-field vortex mode, with  $\alpha$  and  $\beta$  representing the coupling parameters. A weak radiative loss of the near-field vortex mode could be described by Equation (3), and the parameter  $\gamma$  is defined as the attenuation factor of the near-field amplitude.  $\theta$  stands for the phase distribution along the azimuthal direction of near-field EM vortex. For simplicity, the coupling between the spoof SPPs waveguide and meta-particle is lossless, which means  $\alpha^2 + \beta^2 = 1$ , the normalized transmission coefficient ( $|E_2|/|E_1|$ ) and relative phase difference ( $\text{Arg}(E_2/E_1)$ ) originated from the particle-waveguide coupling process can be given as the following Equations (4) and (5), respectively.

$$\frac{|E_2|}{|E_1|} = \sqrt{\frac{(1 - \gamma)^2 + \alpha^2 - 2(1 - \gamma)\alpha\cos\theta}{1 + (1 - \gamma)^2\alpha^2 - 2(1 - \gamma)\alpha\cos\theta}} \quad (4)$$

$$\text{Arg}\left(\frac{E_2}{E_1}\right) = \theta - \pi + \text{atan}\frac{\alpha\sin\theta}{1 - \gamma - \alpha\cos\theta} + \text{atan}\frac{(1 - \gamma)\alpha\sin\theta}{1 - (1 - \gamma)\alpha\cos\theta} \quad (5)$$

Considering the weak radiative loss of near-field EM vortex, we select  $\gamma = 0.01$  while  $\alpha = 0.988$  to fit the normalized transmission coefficient and relative phase difference as shown in Figure 4d. The theoretical prediction (in Figure 4d, abscissa  $[\theta]$  close to

$2\pi$ ) and the numerical calculation (in Figure 4c, abscissa [frequency] near 9.9 GHz) unanimously appear strong suppression and an abrupt phase delay about  $2\pi$  for the transmission of spoof SPPs, which indicates the efficient generation of near-field EM vortex mode. In fact, excited by a free space wave, the dipole resonance of the meta-particle (depicted in Figure 1) consists of two degenerate localized vortex modes rotating in the opposite directions. Due to the EM wave with symmetric field illuminating on the meta-particle, these two degenerate vortex modes could be excited simultaneously, which have the same amplitude with complementary topological charges. For the sake of bidirectional oscillation, these two degenerate vortex modes interfere and show the typical field pattern as a dipole resonance, in which the OAM information carried by vortices cancels each other. The corresponding schematic diagram is shown in Figure S9 of the Supporting Information. On the contrary, the asymmetric field provided by the comb-shaped stripe could lead to a unidirectional EM coupling from spoof SPPs waveguide to the meta-particle, and therefore create a localized mode carrying OAM.

## 6. Microwave Experiments for Plasmonic Vortex

The asymmetric spatial distribution of excitation field ensures the effective excitation of near-field EM vortex. To verify our numerical design and the theoretical analysis, the microwave experiments are performed. The geometric parameters of the prepared samples, including the meta-particle and the comb-shaped stripe, are almost the same as our numerical models described before. The details of the samples are shown in Figure S10 of the Supporting Information. The microwave EM responses and the corresponding field distribution as well as the phase distribution are measured by a vector network analyzer (Agilent E5063A). The excitation direction of spoof SPPs is indicated by the red arrow shown in the inset of Figure 5a. The coupling effect between spoof SPPs waveguide and meta-particle can strongly suppress the transmission of spoof SPPs near 9.58 GHz, as demonstrated by the measured transmission ( $S_{21}$ ) and reflection ( $S_{11}$ ) coefficients of the hybrid waveguide combined with meta-particle in Figure 5a. The slight difference of response frequency between the measured and calculated results could be attributed to the geometry deviation of the fabricated sample from the original design. In addition, we succeeded in detecting the additional abrupt phase delay (nearly  $2\pi$ ) for the transmission of spoof SPPs near 9.58 GHz (Figure S11, Supporting Information). Figure 5b shows the measured near-field distribution in the  $x$ - $y$  plane 1 mm above the meta-particle at 9.58 GHz, in which the four snapshots show the dynamic behavior of the counter-clockwise rotating vortex (topological charge  $l = -1$ ). Obvious phase singularity and continuous helical phase distribution along the azimuthal direction are observed in Figure 5c. The measurement results for clockwise localized vortex (topological charge  $l = +1$ ) are shown in Figure S12 of the Supporting Information.

## 7. Conclusion

In summary, based on the full-wave numerical simulations and theoretical analyses, we propose an effective way to gene-

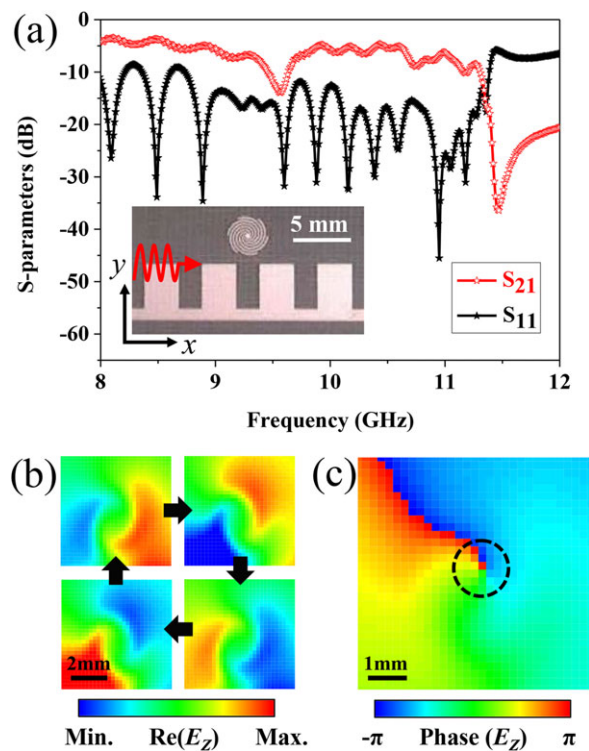


**Figure 5.** Experimental verification of counter-clockwise localized vortex (topological charge  $l = -1$ ). a) Red and black lines represent the measured transmission ( $S_{21}$ ) and reflection ( $S_{11}$ ) coefficient of the hybrid waveguide combined with meta-particle, respectively. The inset is the photograph of the fabricated sample. b) Measured near-field distribution and c) helical phase distribution of  $E_z$  component for counter-clockwise vortex in an  $x$ - $y$  plane (1 mm above the meta-particle) at 9.58 GHz. The four snapshots of the measured near-field distribution (b) are taken at every quarter of a period.

tate near-field vortex modes at low frequencies. The system is composed of a metal spiral meta-particle and a comb-shaped spoof SPPs waveguide. We demonstrate that the plasmonic vortex modes with desired topological charges confined in this deep-subwavelength meta-particle could be effectively excited through the asymmetrical spatial field provided by the spoof SPPs waveguide. The microwave experiments are performed to verify the simulation result and theoretical predictions. Generating plasmonics-like EM vortices at a deep-subwavelength scale, our proposed method breaks the high frequency limitation of plasmonic vortices, which may find potential applications in integrated EM devices in microwave and terahertz frequencies.

## Supporting Information

Supporting Information is available from the Wiley Online Library or from the author.

## Acknowledgements

H.S. and X.S. contributed equally to this work. This work was financially supported by National Key R&D Program of China (No. 2017YFA0303702) and National Natural Science Foundation of China (No. 11674166,

11621091, 61372048, 91750202, 11474156, and 11574270). Y. L. acknowledges the financial support from National Science Foundation under grant number DMR-1654192.

## Conflict of Interest

The authors declare no conflict of interest.

## Keywords

deep-subwavelength, metamaterials, orbital angular momentum, plasmonic vortices

Received: January 10, 2018

Revised: May 9, 2018

Published online:

- 
- [1] M. Onoda, S. Murakami, N. Nagaosa, *Phys. Rev. Lett.* **2004**, *93*, 083901.
- [2] X. Yin, Z. Ye, J. Rho, Y. Wang, X. Zhang, *Science* **2013**, *339*, 1405.
- [3] L. Allen, M. W. Beijersbergen, R. J. C. Spreeuw, J. P. Woerdman, *Phys. Rev. A* **1992**, *45*, 8185.
- [4] A. E. Willner, H. Huang, Y. Yan, Y. Ren, N. Ahmed, G. Xie, C. Bao, L. Li, Y. Cao, Z. Zhao, J. Wang, M. P. J. Lavery, M. Tur, S. Ramachandran, A. F. Molisch, N. Ashrafi, S. Ashrafi, *Adv. Opt. Photonics* **2015**, *7*, 66.
- [5] A. M. Yao, M. J. Padgett, *Adv. Opt. Photonics* **2011**, *3*, 161.
- [6] M. Padgett, R. Bowman, *Nat. Photonics* **2011**, *5*, 343.
- [7] S. Bernet, A. Jesacher, S. Furrhapter, C. Maurer, M. Ritsch-Marte, *Opt. Express* **2006**, *14*, 3792.
- [8] A. Nicolas, L. Veissier, L. Giner, E. Giacobino, D. Maxein, J. Laurat, *Nat. Photonics* **2014**, *8*, 234.
- [9] J. Wang, J. Y. Yang, I. M. Fazal, N. Ahmed, Y. Yan, H. Huang, Y. Ren, Y. Yue, S. Dolinar, M. Tur, A. E. Willner, *Nat. Photonics* **2012**, *6*, 488.
- [10] G. Vallone, V. D'Ambrosio, A. Sponselli, S. Slussarenko, L. Marucci, F. Sciarrino, P. Villoresi, *Phys. Rev. Lett.* **2014**, *113*, 060503.
- [11] K. D. Wulff, D. G. Cole, R. L. Clark, R. DiLeonardo, J. Leach, J. Cooper, G. Gibson, M. J. Padgett, *Opt. Express* **2006**, *14*, 4169.
- [12] A. Jesacher, A. Schwaighofer, S. Furrhapter, C. Maurer, S. Bernet, M. Ritsch-Marte, *Opt. Express* **2007**, *15*, 5801.
- [13] G. Gibson, J. Courtial, M. J. Padgett, M. Vasnetsov, V. Pas'ko, S. M. Barnett, S. Franke-Arnold, *Opt. Express* **2004**, *12*, 5448.
- [14] N. Yu, P. Genevet, M. A. Kats, F. Aieta, J. P. Tetienne, F. Capasso, Z. Gaburro, *Science* **2011**, *334*, 333.
- [15] Y. Yang, W. Wang, P. Moitra, I. I. Kravchenko, D. P. Briggs, J. Valentine, *Nano Lett.* **2014**, *14*, 1394.
- [16] E. Karimi, S. A. Schulz, I. De Leon, H. Qassim, J. Upham, R. W. Boyd, *Light Sci. Appl.* **2014**, *3*, e167.
- [17] M. I. Shalaev, J. Sun, A. Tsukernik, A. Pandey, K. Nikolskiy, N. M. Litchinitser, *Nano Lett.* **2015**, *15*, 6261.
- [18] X. Cai, J. Wang, M. J. Strain, B. Johnson-Morris, J. Zhu, M. Sorel, J. L. O'Brien, M. G. Thompson, S. Yu, *Science* **2012**, *338*, 363.
- [19] P. Miao, Z. Zhang, J. Sun, W. Walasik, S. Longhi, N. M. Litchinitser, L. Feng, *Science* **2016**, *353*, 464.
- [20] G. Spektor, D. Kilbane, A. K. Mahro, B. Frank, S. Ristok, L. Gal, P. Kahl, D. Podbiel, S. Mathias, H. Giessen, F. J. Meyer zu Heringdorf, M. Orenstein, M. Aeschlimann, *Science* **2017**, *355*, 1187.
- [21] Y. Gorodetski, A. Niv, V. Kleiner, E. Hasman, *Phys. Rev. Lett.* **2008**, *101*, 043903.
- [22] H. Kim, J. Park, S. W. Cho, S. Y. Lee, M. Kang, B. Lee, *Nano Lett.* **2010**, *10*, 529.
- [23] W. Y. Tsai, J. S. Huang, C. B. Huang, *Nano Lett.* **2014**, *14*, 547.
- [24] C. F. Chen, C. T. Ku, Y. H. Tai, P. K. Wei, H. N. Lin, C. B. Huang, *Nano Lett.* **2015**, *15*, 2746.
- [25] S. Y. Lee, S. J. Kim, H. Kwon, B. Lee, *IEEE Photonics Technol. Lett.* **2015**, *27*, 705.
- [26] J. B. Pendry, L. Martin-Moreno, F. J. Garcia-Vidal, *Science* **2004**, *305*, 847.
- [27] F. J. Garcia-Vidal, L. Martin-Moreno, J. B. Pendry, *J. Opt. A: Pure Appl. Opt.* **2005**, *7*, S97.
- [28] A. Pors, E. Moreno, L. Martin-Moreno, J. B. Pendry, F. J. Garcia-Vidal, *Phys. Rev. Lett.* **2012**, *108*, 223905.
- [29] S. A. Maier, S. R. Andrews, L. Martin-Moreno, F. J. Garcia-Vidal, *Phys. Rev. Lett.* **2006**, *97*, 176805.
- [30] D. Martin-Cano, M. L. Nesterov, A. I. Fernandez-Dominguez, F. J. Garcia-Vidal, L. Martin-Moreno, E. Moreno, *Opt. Express* **2010**, *18*, 754.
- [31] X. Shen, T. J. Cui, D. Martin-Cano, F. J. Garcia-Vidal, *Proc. Natl. Acad. Sci. USA* **2013**, *110*, 40.
- [32] H. F. Ma, X. Shen, Q. Cheng, W. X. Jiang, T. J. Cui, *Laser Photonics Rev.* **2014**, *8*, 146.
- [33] P. A. Huidobro, X. Shen, J. Cuerda, E. Moreno, L. Martin-Moreno, F. J. Garcia-Vidal, T. J. Cui, J. B. Pendry, *Phys. Rev. X* **2014**, *4*, 021003.
- [34] X. Shen, T. J. Cui, *Laser Photon. Rev.* **2014**, *8*, 137.
- [35] Z. Gao, F. Gao, Y. Zhang, X. Shi, Z. Yang, B. L. Zhang, *Appl. Phys. Lett.* **2015**, *107*, 041118.
- [36] Z. Gao, F. Gao, Y. Zhang, B. L. Zhang, *Appl. Phys. Lett.* **2015**, *107*, 191103.
- [37] Z. Liao, X. Shen, B. C. Pan, J. Zhao, Y. Luo, T. J. Cui, *ACS Photon.* **2015**, *2*, 738.
- [38] J. Petersen, J. Volz, A. Rauschenbeutel, *Science* **2014**, *346*, 67.
- [39] P. Wang, Y. Wang, Z. Yang, X. Guo, X. Lin, X. C. Yu, Y. F. Xiao, W. Fang, L. Zhang, G. W. Lu, Q. H. Gong, L. M. Tong, *Nano Lett.* **2015**, *15*, 7581.
- [40] A. Yariv, *Electron. Lett.* **2000**, *36*, 321.
- [41] J. E. Heebner, V. Wong, A. Schweinsberg, R. W. Boyd, D. J. Jackson, *IEEE J. Quantum Electron.* **2004**, *40*, 726.
- [42] J. E. Heebner, R. W. Boyd, *Opt. Lett.* **1999**, *24*, 847.